Magnetic Suspension and Vibration Control of Beams for Non-contact Processing

David L. Trumper, Associate Professor
Ming-chih Weng, Research Assistant
Robert J. Ritter, Research Assistant
Department of Mechanical Engineering
Massachusetts Institute of Technology
Cambridge, MA, USA

Abstract

This paper presents an integrated approach to magnetic suspension of a tubular beam for non-contact processing. We describe non-contact sensors and actuators, structure modelling/identification, and control methods for such systems. We have also designed an experiment that uses 8 sensors and 8 actuators to suspend a 3 m long, 6.35 mm diameter steel tube. Results from this experiment are presented herein. To facilitate the experiment, we designed a novel two-dimensional position sensor by utilizing the concept of an x-y variable differential transformer. We also designed two types of actuators that apply magnetic force on the tube in two axes. The system dynamics are modelled theoretically, and identified experimentally from within the closed-loop system. In order to control the system under varying boundary conditions, we propose a *slow roll-up* lead compensator. We also introduce sensor interpolation and sensor averaging methods to make the control loop more robust. Our proposed ideas are verified in the experimental results.

1. Introduction

Many industrial operations center on the processing of an elongated element moving axially through successive functional stations. Examples include steel rolling, plastic film production, paper production, coating, and painting. In these processes it may be advantageous to be able to handle the product without directly touching it. The work described herein grows out of the idea developed by Dr. Conrad Smith [1] for the production of painted metal handles for brooms and mops. The idea developed by Dr. Smith is shown schematically in Figure 1. The first author served as a consultant to Dr. Smith in developing this process, which has been successfully used to produce finished handles. This paper builds on this work by

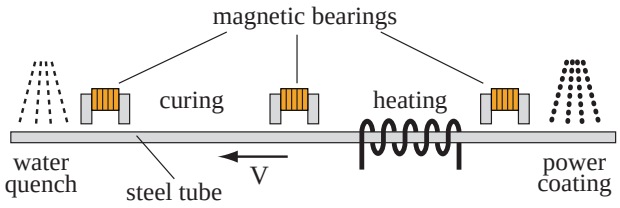

Figure 1: Non-contact coating process

presenting general theory for magnetic suspension of tubular beams for non-contact processing. Our work builds on the fields of magnetic suspension [2][3] and vibration control [4]. We integrate these technologies and present general results to support non-contact processing systems. Our experimental setup is shown in Figure 2. We use 8 sensors and 8 actuators to suspend a 3 m long, 6.35 mm diameter steel tube.

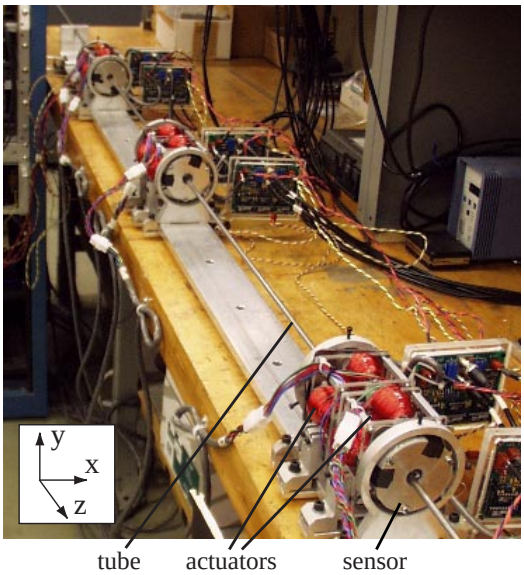

Figure 2: Experimental setup

2. Background

2.1. Structural Dynamics

The suspended tube is well modelled as a Euler-Bernoulli Beam moving with axial velocity V. Assuming constant bending stiffness EI and axial tension force T, the governing equation can be derived as

$$EI\frac{\partial^4 u}{\partial z^4} - T\frac{\partial^2 u}{\partial z^2} + \rho A\frac{\partial^2 u}{\partial t^2} + 2\rho A\frac{\partial^2 u}{\partial z \partial t}V + \rho A\frac{\partial^2 u}{\partial z^2}V^2 = f. \quad (1)$$

Here z is axial axis, u is transverse deformation, ρ is material density, A is cross-sectional area, and f is transverse force density. Equation(1) represents a linear gyroscopic system; here the last 2 terms represent Coriolis force and centripetal force due to axial motion, respectively. In this paper, we neglect T and V and use the simpler stationary beam model

$$EI\frac{\partial^4 u}{\partial z^4} + \rho A\frac{\partial^2 u}{\partial t^2} = f. \quad (2)$$

This equation can be further decoupled and truncated into finite number of decoupled mode equations. We add a constant damping ratio $\zeta = 0.005$ into each mode to complete the modelling.

To verify if the velocity V is negligible, we compare V with the critical speed V_c, which is the lowest speed at which divergence instability happens. For a beam with length L, the critical speed is [5]:

$$\begin{cases} V_c = \sqrt{\frac{T}{\rho A} + \pi^2 \frac{EI}{\rho A L^2}} & \text{simple supports} \\ V_c = \sqrt{\frac{T}{\rho A} + 4\pi^2 \frac{EI}{\rho A L^2}} & \text{fixed supports} \end{cases} \quad (3)$$

For our system with simple supports, given the tube parameters, the critical speed can be obtained as $V_c = 10$ m/s. If the object is moving at speed close to or higher than V_c, (1) should be used to model the structure. If desired, a finite element model can be derived directly from the governing equation; the modal analysis techniques we've used can be found in references [6][7].

2.2. Electromagnetic Theories

Electromagnetic analysis presented in [8][9] are essential to design the magnetic actuators and sensors. For small air gaps, a magnetic circuit model is suitable to predict the system performance. For large air gaps, the result is more accurate by solving the magnetic field from Laplace's equation (low frequency) or the magnetic diffusion equation (high frequency).

2.2.1 Actuators: Due to the low bandwidth, the performance of the actuators can be predicted by a quasi-static low-frequency field analysis. At first, the magnetic scalar potential Ψ can be solved via Laplace's equation

$$\nabla^2 \Psi = 0 \quad (4)$$

along with appropriate boundary conditions. Since steel has a permeability of about $10^4 \mu_o$, we can consider Ψ constant on the steel tube, and the magnetic field is thus perpendicular to the tube surface. The magnetic field intensity $\vec{H}$ can be obtained from Ψ by

$$\vec{H} = -\nabla \Psi. \quad (5)$$

Once $\vec{H}$ is calculated (either from a magnetic circuit model or Laplace's equation), the force density $\vec{f}$ on the tube can be calculated from $\vec{H}$. Since the magnetic field has only perpendicular component $H_\perp$ on the tube, there is only a normal force $f_\perp$ on the tube surface

$$df_\perp = \frac{1}{2}\mu_o H_\perp^2 dA, \quad (6)$$

where $df_\perp$ is the force acting on an area element dA.

2.2.2 Sensors: To predict the sensor performance, since the sensor operates at the relatively high frequency of 6 kHz, we consider the ac field effect by introducing the magnetic diffusion equation

$$\nabla^2 \vec{H} = \mu\sigma\frac{\partial \vec{H}}{\partial t}. \quad (7)$$

We can either solve the magnetic diffusion equation, or use a modified magnetic circuit model by introducing the concept of skin depth. While applying an ac magnetic field, the tube attracts the magnetic field a certain skin depth δ into the material, where

$$\delta = \sqrt{\frac{2}{\mu\sigma\omega}}. \quad (8)$$

The three variables here are permeability μ, conductivity σ, and the ac field frequency ω. Once δ is known, we can solve magnetic circuit model by using δ as the equivalent material thickness.

3. Experimental Setup

As shown in Figure 2, we use 8 sensors and 8 actuators to suspend the steel tube. Both sensors and actuators have 12.7 mm bores. The tube has density $\rho = 7800$ Kg/m^3, Young's Modulus $E = 200$ GPa, outside diameter $\phi = 6.35$ mm, wall thickness $w = 0.89$ mm, cross-sectional area $A = 15.3$ mm^2, moment of inertia $I = 58.4$ mm^4, and length $L = 3$ m. The experiment controller is implemented on a digital signal processing (DSP) board with a sampling

time of 500 μs. In the following sections, we discuss details of the associated sensor and actuator design, as well as the control system designs and associated experimental results.

4. Sensor Design

A sensor used in non-contact processing needs to be robust with respect to surface coatings and dusty environments. It also needs a large air gap to allow possible beam vibration, as well as having a small axial length in order to be placed close to the actuator in order to avoid non-collocation problems. We have designed a non-contact position sensor compatible with the magnetic suspension process [10], as shown in Figure 3. This sensor works as a two dimensional variable differential transformer.

Figure 3: Two dimensional variable differential transformer sensor

The schematic design is shown in Figure 4. The three primary coils on the sensor poles are the inputs driven by 6 kHz sinusoidal three-phase excitation currents. The three secondary coils are the outputs that read the time derivative of magnetic flux linkage $V = -\dot{\lambda}$. The x and y positions are obtained by synchronously detecting the output voltages V_a, V_b and V_c as

$$V_x = \sqrt{3}(V_a sgn(I_3) - V_c sgn(I_2))H_L(s) \quad (9)$$

$$V_y = (2V_b sgn(I_1) - V_a sgn(I_3) - V_c sgn(I_2))H_L(s). \quad (10)$$

Here $sgn(u)$ is the signum function equal to ± 1 depending on the sign of u , and $H_L(s)$ is a 4^{th} order low-pass filter with 1 kHz bandwidth. The experimentally-measured sensor output is shown in Figure 5, compared with our theoretical result. It shows the sensor output V_x and V_y when the tube is moving in a 1 mm grid.

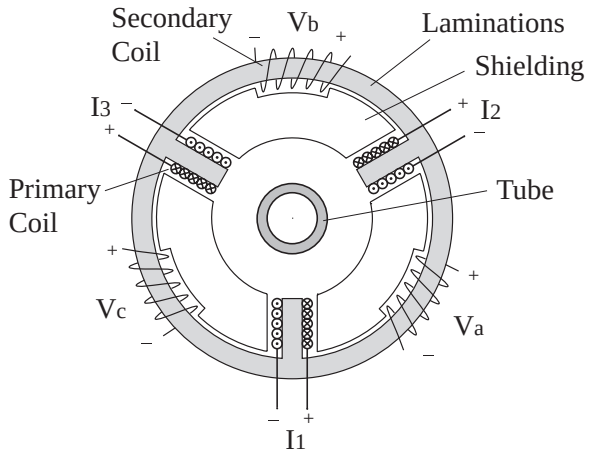

Figure 4: Sensor schematic design

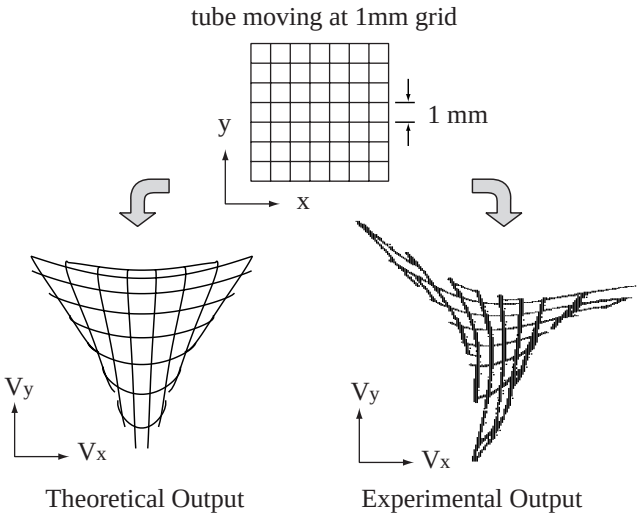

Figure 5: Sensor output grid

5. Actuator Design

We have designed two types of actuators, a dipole-quadrupole actuator and a quad-U-core actuator, and have compared their performances theoretically and experimentally. Both their force capacities are limited by heat transfer and by magnetic saturation.

5.1. Dipole-Quadrupole Actuator

The dipole-quadrupole actuator is shown in Figure 6. Picture (a) shows 12 poles of the actuator and the top half of the dipole coil, and picture (b) shows the completed actuator. The dipole-quadrupole field theory is illustrated in Figure 7. The actuator uses 12 poles to simulate a sinusoidal current distribution. It generates a dipole field, an x quadrupole field, and an y quadrupole field. The dipole generates a uniform field and thereby magnetizes the tube with a magnetization vector $\vec{m}$. The quadrupoles generate gradient

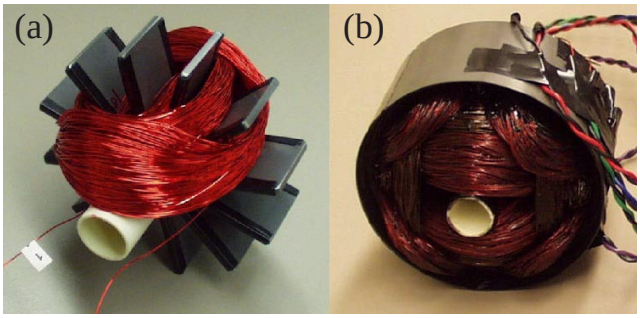

Figure 6: Dipole-quadrupole actuator: (a)dipole coil winding, (b)completed actuator

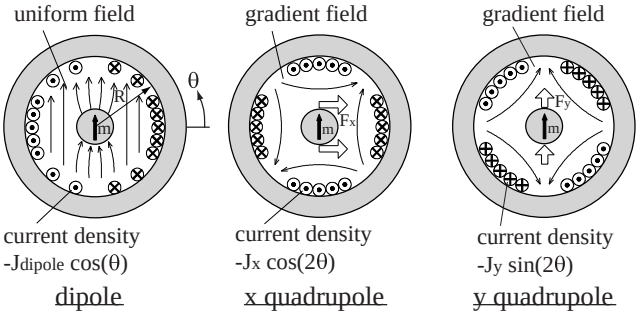

Figure 7: Theory of dipole-quadrupole actuator

fields which interact with $\vec{m}$ and thereby generate net force on the magnetized tube. The field intensities are

$$\vec{H}_{dipole} = J_{dipole}\hat{e_x} \quad (11)$$

$$\vec{H}_{quad,x} = J_x\frac{y}{R}\hat{e_x} + J_x\frac{x}{R}\hat{e_y} \quad (12)$$

$$\vec{H}_{quad,y} = J_y\frac{x}{R}\hat{e_x} + J_y\frac{y}{R}\hat{e_y}. \quad (13)$$

The resulting force can be predicted by the Kelvin magnetization force density as

$$\vec{f} = \mu_o\vec{m}\cdot\nabla\vec{H}. \quad (14)$$

Hence by keeping the dipole field constant, ideally, this actuator will have force as a linear function of input current and independent of the tube position:

$$f_x = \mu_o m\frac{J_x}{R} \quad (15)$$

$$f_y = \mu_o m\frac{J_y}{R} \quad (16)$$

By solving for the magnetic field (using Laplace's equation), we can predict the actuator performance. The result is shown in Figure 8 compared with the experimental result. The disagreement is believed to be mainly due to the saturation of the actuator poles.

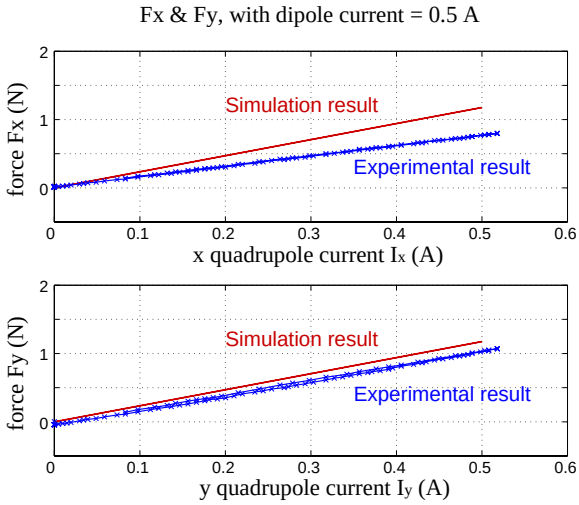

Figure 8: Force versus current of the dipole-quadrupole actuator with the tube centered

This actuator has the advantage that F_x and F_y are decoupled. However, while the data is not shown here, the force is dependent on the tube position. The main disadvantage of this actuator is that, since the dipole is not perfect, the tube tends to stick to the pole pieces if allowed to move too far from the centered position. A practical problem is that the actuator is difficult to build, since the coils need to be wound by hand in a built-up fashion.

5.2. Quad-U-Core Actuator

The difficulties mentioned above led us to design another type of actuator as shown in Figure 9(a). This actuator consists of 4 U-core electromagnets to control the $\pm x$ and $\pm y$ direction forces. Figure 9(b) shows a single U-core electromagnet.

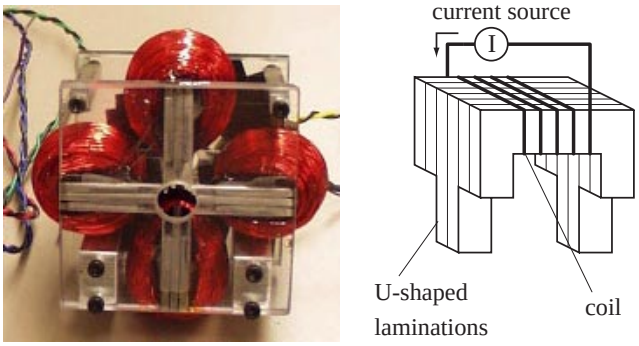

Figure 9: (a)Quad-U-core actuator, (b)schematic design of a single U-core electromagnet

It has the advantage that it is easy to build. A disadvantage is that F_x and F_y are coupled in the way

that they are functions of both current inputs, in other words, $F_x = F_x(i_x, i_y)$ and $F_y = F_y(i_x, i_y)$. Another disadvantage is that the force-current relation is nonlinear. The current-force function in each U-core electromagnet is measured to be

$$F(N) = 30\frac{I^2}{g^2}. \tag{17}$$

Here I is the coil current input in A, and g is the air gap in mm. The theoretical result agrees with this result within 20% error. We can linearize the force-current relation by either putting bias current on each U-core, or using feedback linearization. Using bias current is similar to adding a permanent magnet, which makes the controller design more difficult since it decreases the suspension unstable time constant [11]. In this paper, we use the feedback linearization method.

6. System Modelling and Identification

6.1. System Modelling

We develop a model of the system by including sensor, actuator, time delay, and structure dynamics. The sensor dynamics result from its low-pass filter with 1 kHz bandwidth. The actuator dynamics are dominated by low-pass filter in the current source controller. A time delay results from the computation time T_s of the controller. Since the control calculations absorb almost a whole sampling interval, a delay of $1.5T_s$ is included in the model to represent this delay plus the zero-order-hold. The structure dynamics can be obtained by either an analytical model or a finite element model. In the work reported herein, we use 100 states to represent the system, and assume a damping ratio $\zeta = 0.005$.

6.2. System Identification

To measure the plant dynamics, we designed a stabilizing controller $H(s)$ and closed the loop as shown in Figure 10. With the swept sine input, we can measure V_1 and V_2 experimentally.

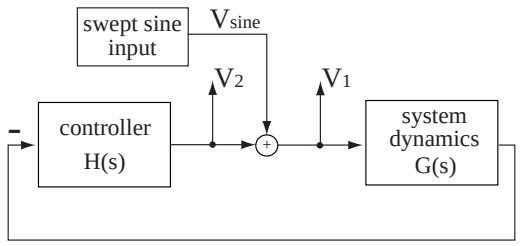

Figure 10: Measure loop transfer function

V_1 and V_2 are:

$$V_1(s) = \frac{1}{1 + H(s)G(s)}V_{sine}(s) \tag{18}$$

$$V_2(s) = \frac{-H(s)G(s)}{1 + H(s)G(s)}V_{sine}(s). \tag{19}$$

Hence the loop transfer function $H(s)G(s)$ can be obtained as

$$H(s)G(s) = -\frac{V_2(s)}{V_1(s)}. \tag{20}$$

7. Control

The challenges of controlling this system result from the following facts:

1. The structure has a low damping ratio $\zeta \approx 0.005$, and thus the modes create large peaks in the transfer function.

2. Because of the sensor low-pass filter, actuator low-pass filter, and time delay, this system has significant phase lag within the control bandwidth.

3. The dereverberated backbone of the plant transfer function falls off only as $\omega^{-1.5}$, Thus it is hard to add lead compensation without introducing instability in the higher modes.

In this paper, we propose three ideas for solving this magnetic suspension control problem.

7.1. Slow Roll-Up Lead Compensator

To deal with the lightly-damped vibration modes, we design a SISO multiple-lead compensator. This compensator has the following structure:

$$H(s) = K_p\frac{(s+m)(s+4m)(s+16m)\cdots}{(s+2m)(s+8m)(s+32m)\cdots} \tag{21}$$

This controller will provide phase margin of about 30 degrees for the frequencies of interest. It has gain rolling up at an average slope of 10dB/decade to avoid over-amplifying resonance peaks at high frequencies.

7.2. Sensor Interpolation

We use 2 sensors and 2 actuators as a package, as shown in Figure 11. We put sensors and actuators close together, and interpolate sensor outputs to obtain the real positions at the actuators. By doing so, we can avoid the sensor/actuator non-collocation problem.

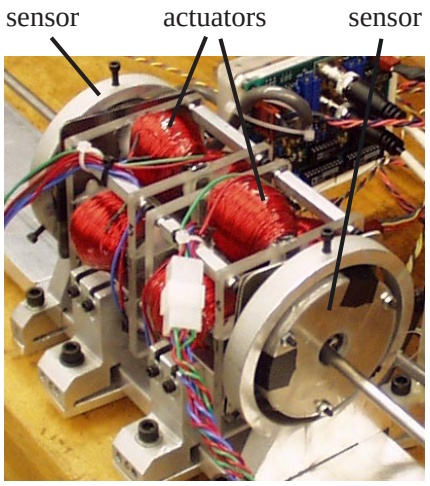

Figure 11: Sensor interpolation

7.3. Sensor Averaging

We place 2 sensors apart to predict the position in the middle. In this configuration, we assume the beam is vibrating as a stationary sinusoidal wave (neglect the evanescent terms $e^{\pm\lambda z}$)

$$u(z,t) = cos(\omega t)cos(\lambda z). \tag{22}$$

Here ω is the natural frequency, and $\lambda = 2\pi/l$ is the spatial wavenumber. In the beam analysis, neglecting T and V, we have

$$EI\lambda^4 = \rho A\omega^2. \tag{23}$$

With sensors located at $z_1 = (z_o - d)$ and $z_2 = (z_o + d)$, the average output is thus given by

$$\begin{aligned} u_{ave}(z_o,t) &= \frac{1}{2}(u(z_1,t) + u(z_2,t)) \\ &= cos(\omega t)cos(\lambda z_o)cos(\lambda d) \\ &= u(z_o,t)cos(\lambda d) \end{aligned} \tag{24}$$

The cosine effect $cos(\lambda d)$ is shown in Figure 12. The result is obtained when $z_o = 1.12$m and $d = 0.15$m. The $cos(\lambda d)$ term creates an ideal low-pass within a certain frequency range without losing phase. If we put the cosine notch at a troubling frequency region (gain $>$ 0dB, phase $< -180^o$), we can reduce the loop gain in this region without adversely affecting the phase, and thereby make the system stable or increase the gain margin.

8. Experimental Result

In this section, we show experimental results taken with local control of the actuator pair shown in Figure 11. In this work, the two actuators are driven as a single source of force.

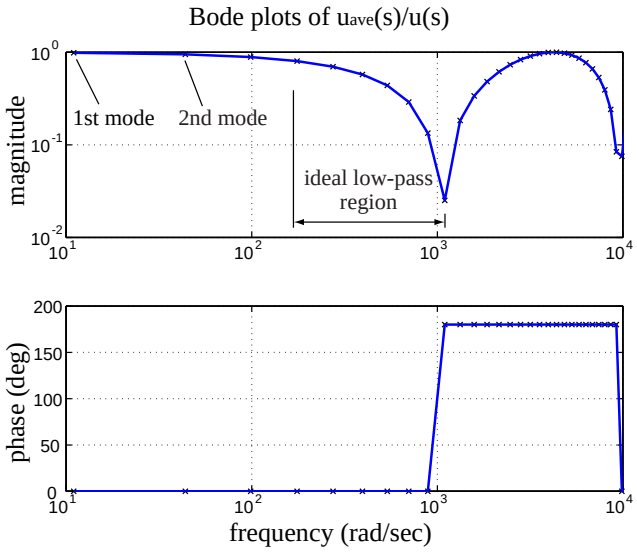

Figure 12: Cosine effect from sensor averaging

8.1. Control with Sensor Interpolation

We clamp the beam at both ends, place sensors and actuators in close proximity (sensor interpolation). We can thus regard a sensor and an actuator as both at $z = 1.12$m. Using the controller

$$H(s) = 4\frac{(s+30)(s+120)(s+400)^2}{(s+60)(s+240)(s+800)^2} \tag{25}$$

we are able to stabilize the system locally, except there is a limit cycle vibration at 1100 rad/s. The measured loop dynamics are shown in Figure 13 compared with our theoretical model.

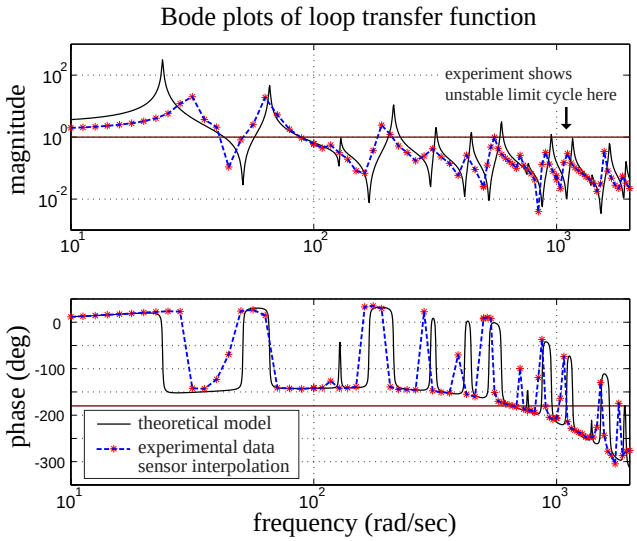

Figure 13: Bode plots of loop transfer function, theoretical and experimental for sensor interpolation

The loop has 30° phase margin for all vibration modes

below 500 rad/s. The alternating pole-zero pattern shows that the modal controllability and modal observability have the same sign [12], which implies there is no non-collocation problem. However, there is an unstable limit cycle vibration at frequency of 1100 rad/s, and we can see the phase at that frequency drops below $-180°$.

8.2. Control with Sensor Averaging

In this section, we pull the sensors apart to implement sensor averaging. Specifically, the sensors are spaced ± 0.15m from the actuator at $z = 1.12$m. We use the same controller as in the previous section. Figure 14 shows the loop transfer function compared between sensor interpolation and sensor averaging. The sensor averaging shows the improvement of gain margin within frequency range from 700 rad/s to 1500 rad/s while the phase is below $-180°$. Thus we are able to stabilize the system and avoid the limit cycle shown in the sensor interpolation experiment.

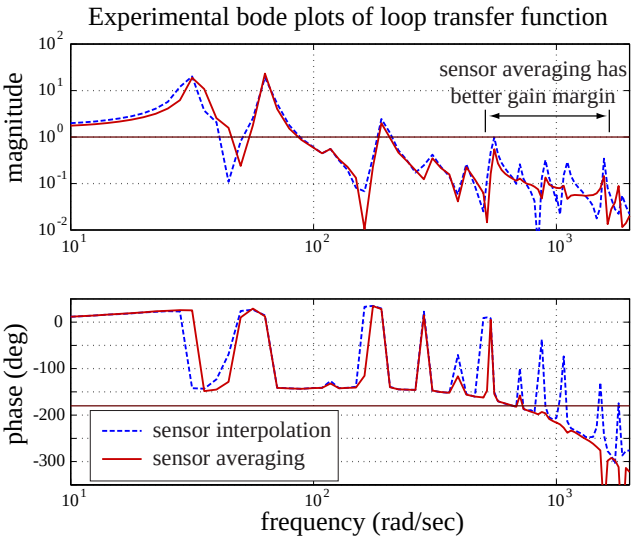

Figure 14: Bode plots of loop transfer function, sensor interpolation and sensor averaging

9. Conclusions

This paper presents an approach to actuator, sensor, and controller design for magnetic suspension of tubular beams for non-contact processing. At the present time, we have focused on using a local control method. We will continue the work on sensor/actuator positioning and control algorithm to reach better performance. We will further explore suspension control with multiple sensors and actuators. We expect this research to lead to new approaches for magnetic suspension for non-contact processing. In the future, we also plan to investigate the dual problem of electrostatic levitation.

10. Acknowledgments

This research is sponsored by the National Science Foundation under Grant Award Number DMI-9700973.

References

[1] American Metal Handle, Vulcan Dr., Birmingham, AL, USA.

[2] "Fourth International Symposium on Magnetic Suspension Technology," NASA, 1998.

[3] "Sixth International Symposium on Magnetic Bearings," MIT, 1998

[4] "Active Control of Vibration and Noise," ASME International Mechanical Engineering Congress and Exposition, 1996.

[5] J.A. Wickert, et al., "Classical Vibration Analysis of Axially Moving Continua," Journal of Applied Mechanics, Transactions of the ASME, Vol. 57, pp.738-744, September 1990

[6] L. Meirovitch, "Elements of Vibration Analysis," McGraw-Hill, 2nd edition, 1986.

[7] L. Meirovitch, "A Modal Analysis for the Response of Linear Gyroscopic Systems," Journal of Applied Mechanics, Transactions of the ASME, pp.446-450, June 1975

[8] H.A. Haus, et al., "Electromagnetic Fields and Energy," Prentice Hall 1989

[9] H.H. Woodson, et al., "Electromechanical Dynamics, Part II: Fields, Forces, and Motion," Robert E. Krieger Publishing 1968

[10] R.J. Ritter, "Analysis and Design of a Two-Axis Noncontact Position Sensor," Master's Thesis, MIT Dept. of Mechanical Engineering, Feb. 1999.

[11] D.L. Trumper, "Magnetic Suspension Techniques for Precision Motion Control," Ph.D. Thesis, MIT Dept. of Electrical Engineering and Computer Science, Sep. 1990.

[12] E.E. Crawley, "16.243 Dynamics of Controlled Structures," MIT course handout, Chapter 6, 1997.